Published November 10, 2016

Journal of Environmental Quality SHORT COMMUNICATIONS

Visualization of Colloid Transport Pathways in Mineral Soils Using Titanium(IV) Oxide as a Tracer

Stefan Koch,* Petra Kahle, and Bernd Lennartz

Abstract

In soils, colloidal transport has been identified as the most important pathway for strong adsorbing, environmental contaminants like pesticides, heavy metals, and phosphorus. We conducted a comparative dye tracer experiment using a Brilliant Blue (BB) solution and a Titanium(IV) oxide (TiO_2) colloid suspension (average particle size 0.3 μm), aiming to visualize and quantify colloid pathways in soils. Both dye tracers showed comparable general flow patterns with preferred transport over the deepest part of the soil profile, independent of clay content. The stained area was generally smaller for TiO_2 than for BB by a factor of ten, however, and there was no TiO_2 to be found at all in the low clay content soil. The travel distance was almost identical for the solution and the suspension (0.7 m) giving evidence that environmentally critical compounds bound to microparticles may be vertically transported over longer distances in soils, even within single rainfall events. The spatial variability of the dye patterns was large on a small scale with a range of 0.35 m for TiO_2 in the horizontal plane, which was taken as a general proof for a pronounced preferential transport situation. The study indicates that TiO_2 is transported exclusively through singular macropores of biogenetic nature, while BB passes also through the soil matrix of coarse-bedded soils, the secondary pore system or interaggregate pore space. The results emphasize the general suitability of TiO_2 for the visualization of colloid transport pathways in soils, opening up new research opportunities for contaminant transport in soils.

Core Ideas

- Colloidal transport is the most important pathway for strong adsorbing contaminants in soils.
- TiO_2 is a suitable tracer to visualize colloid pathways in mineral soils.
- The distribution of colloid dye tracer can be explained as a function of clay and silt content.
- TiO_2 is exclusively transported in singular macropores rather than along soil ped interfaces.

J. Environ. Qual. 45:2053–2059 (2016)
doi:10.2134/jeq2016.04.0131

Received 7 Apr. 2016.
Accepted 26 Aug. 2016.
*Corresponding author (stefan.koch4@uni-rostock.de).

It has been a unanimous doctrine in soil science for a long time that strong adsorbing compounds, such as phosphate, are transported via erosion bound to soil particles (Sharpley and Syers, 1979; Daniel et al., 1994; Sharpley et al., 1994). Recently, there occurred increasing evidence that colloids are also transported vertically through the soil. The particle-facilitated transport has been identified as important pathway for the leaching of contaminants like pesticides, heavy metals, and phosphorous (P) (Jacobsen et al., 1997; de Jonge et al., 2004; Makris et al., 2006). Jiang et al. (2015) investigated the P contents of soil aggregate-sized fractions from <0.45 to >20 μm and found a significant increase of the overall P content with decreasing aggregate-sized fractions. Heathwaite et al. (2005) stated that total and reactive P is favorably transported in fractions of 2 μm, or smaller than 0.001 μm. The authors highlighted the potential of P colloids to be leached out through subsurface drainage by rainfall events.

McGechan and Lewis (2002) reviewed a multitude of research papers and summarized that macropore and preferential flow are the main processes of colloid and particle transport. Although particle transport in soils has often been studied, it is not known as to what extent colloidal transport patterns compare with the travel pathways of dissolved substances. No attempt has been made to visualize the migration of colloids in soils and therewith to obtain further insight into potential contaminant transport.

The application of dye tracers in infiltration experiments aiming at the visualization of transport processes in soils is well established in soil science. For decades, dye tracers have been used to identify flow pathways in different soils and types of land use (Stamm et al., 1998; Janssen and Lennartz, 2008; Kodešová et al., 2015). The list of available dye tracers is long, and the suitability of a specific dye is essentially determined by the research question and the particular experimental constraints.

Brilliant Blue (BB) is a popular dye tracer in soil science due to its nontoxicity, mobility, bright blue color, and nonconservative adsorptive behavior (Morris et al., 2008). The physical and chemical performance of BB was investigated by Flury and Flühler (1995) and Kasteel et al. (2002) in different soils.

Morris et al. (2008) found that the sorption of BB is not fully reversible and suggested that BB is not suitable for all forms of dye tracing in soils. Adsorption of BB to clay colloids substantially increases with increasing clay content and decreasing pH-values. Likewise, an elevated ionic strength of the background solution

S. Koch, P. Kahle, and B. Lennartz, Agricultural and Environmental Sciences, Univ. of Rostock, Justus-von-Liebig-Weg 6, 18059 Rostock, Germany. Assigned to Associate Editor Saeed Torkzaban.

Abbreviations: BB, Brilliant Blue; TiO_2, titanium(IV) oxide.

leads to higher sorption coefficients of BB (Germán-Heins and Flury, 2000). Janssen and Lennartz (2008) found marked amounts of BB solute shifting by preferential flow in paddy rice fields in China, while Chyba et al. (2013) stated that soil compaction significantly affects the infiltration of BB in the topsoil.

Titanium(IV) oxide (TiO_2), also known as titanium dioxide, is a bright white pigment widely used for coloring and varnish and as a food dye. It is not soluble in water and most organic solvents. A broad range of particle sizes are available for different applications. Titanium(IV) oxide was first used by Liu & Lennartz (2015) to visualize preferential colloid pathways in dark-colored peat soils. However, TiO_2 is more recently in the focus of environmental and health sciences due to its potential as a hazardous nanoparticle (Long et al., 2006; Weir et al., 2012; Frazier et al., 2014). Titanium(IV) oxide particles are available in different sizes. It can be assumed that a narrow TiO_2 particle-size distribution with a mean of 0.3 μm is a good representation of naturally occurring soil colloids of that size.

Although the in situ visualization of soil pore distribution is redeemed by high-end laboratory techniques, like X-ray computer tomography (Rogasik et al., 1999; Cnudde et al., 2006), field studies can be a useful tool for understanding soil physical processes at the field and pedon scale. Furthermore, there are limitations of laboratory techniques when it comes to the detection of active pore space in a soil sample. Active pore space, in this context, denotes the pore volume that is available for convective transport processes for the compound of consideration. Thus, dye tracer studies still appear to be an appropriate method, revealing transport mechanisms under field conditions.

The aim of this study was to visualize the colloid transport in three different mineral soils used for crop production along a gradient of increasing clay content in northeastern Germany. In addition, we wanted to uncover differences in transport patterns between real solutions (BB) and suspensions (TiO_2) by analyzing stained soil profiles.

Based on literature studies, we hypothesize (i) that both tracers follow preferential pathways in the soil, (ii) that the penetration depth of the tracer in the soil profile is a function soil texture, and (iii) that TiO_2 is suitable for the visualization of colloid transport in mineral soils and exhibits a behavior that compares with the mobility of naturally occurring soil colloids.

Studies using TiO_2 as a dye tracer in mineral soils are not available. We believe that the higher clay content causes temporal, resistant, singular biogene macropores that can transport the TiO_2 suspension through the soil, while in loose-bedded soils, earthworm holes are not persistent and soil macropores only allow very limited access of colloidal TiO_2.

Materials and Methods

Study Region

The study region was a pleistocene lowland landscape located 10 km southeast of the city of Rostock in the federal state Mecklenburg-Western-Pomerania in northeastern Germany. The landscape is dominated by light hillslopes (average slope class 0–4%, maximum slope class 8–32%) on a ground moraine formed in the Weichselian sequence. The climate is characterized by a gradient from Atlantic to continental, with an annual precipitation of 660 mm and a mean annual temperature of 9.1°C (German Weather Service, normal period 1981–2010).

We conducted the dye tracer experiments on three different soils along a clay content gradient (Table 1). The soil types were a Stagnosol (Aqualf, site S), a Cambisol (Ochrept, site C), and a Regosol (Entisol, site R), according to FAO (IUSS Working Group WRB, 2015 [USDA taxonomy in brackets; Soil Survey Staff, 1999]). These soil types are typical for the lowlands in northeastern Germany formed on Pleistocene glacial till. The A horizon had a thickness of 0.3 m at the sites C and R. Deep plowing in a 5-yr cycle at site S had caused the formation of a secondary A horizon.

The study sites S and C were intensively used agricultural acreages with sugar beet (*Beta vulgaris* L.) in 2015, and the site R was a 1 yr abandoned field with dry grassland vegetation.

Experimental Design

We conducted dye tracer experiments with BB and TiO_2 (Tiona AT-1, Cristal Global, average particle size 0.3 μm with 75% of the particles being in the range of 0.2–0.4 μm [information supplied by Cristal Global]). A metal collar sized 0.7 × 0.7 m was carefully inserted into the soil (0.03 m depth). Twenty-four and a half liters (50 mm) of water with a BB concentration of 4 g L^{-1} (as suggested by Flury et al., 1994), or a concentration of 10 g L^{-1} TiO_2 (as suggested by Liu and Lennartz, 2015), were slowly poured out of a polyvinyl chloride canister onto a plastic sheet that covered the soil within each collar. The plastic sheet was then carefully (slowly, from one side to the other within 5–10 s) removed to ensure uniform flooding conditions. Twenty-four hours later, eight vertical soil profiles with a spacing of 0.1 m were prepared successively by sidewise cutting the soil with a spade at each experimental site and photographed. The soil pit was 2 m wide and 1 m deep to allow photographing of both (BB and TiO_2) infiltration domains. The photo-documented area of each soil profile was 0.49 m^2 (0.7 × 0.7 m) for each dye tracer. In total, 48 soil profiles (three sites × eight profiles × two dye tracers) were prepared and processed—24 profiles with BB and 24 with TiO_2.

To determine the standard soil physical properties of the experimental sites, disturbed and undisturbed soil samples were taken horizonwise. Undisturbed samples were collected using 5 stainless steel cylinders of approximately 250 cm^3 of volume (7.1 cm in diameter and 6.2 cm in length) at each horizon. Disturbed samples were taken according to a randomly distributed pattern over each horizon. Particle size distribution (<2 mm) was determined using a combined sieve and pipette method (Deutsches Institut für Normung, 2011). The water retention function was measured using ceramic suction plates (at pF 1.8 and 2.48, corresponding to 60 and 300 hPa) and a pressure membrane apparatus (at pF 4.2, corresponding to 15000 hPa). The water retention curve allowed calculating various pore size classes:

macropores (MaP) > 50 μm; MaP = total porosity − θ at 60 hPa

mesopores (MeP) = 50 to 0.2 μm; MeP = θ at 60 hPa − θ at 15000 hPa

micropores (MiP) < 0.2 μm; MiP = θ at 15000 hPa

where θ is the volumetric water content (% volume).

Table 1. Physical characteristics of the soils at the study sites.

Site	Depth	Clay (≤2 μm)	Silt (2–63 μm)	Sand (63–2000 μm)	Stones	Micropores (≤0.2 μm)	Mesopores (0.2–50 μm)	Macropores (>50 μm)	Bulk density	Organic matter content	Munsell soil color
	m	%				% volume			g cm^{-3}	%	
S	0.00–0.30	7.6	48.5	43.6	0.3	7.6 ± 1.77	24.9 ± 4.29	13.5 ± 2.1	1.44 ± 0.32	2.0–4.0	10YR 3/3
	0.30–0.42	8.4	47.4	43.8	0.4	7.6 ± 0.09	20.7 ± 0.49	12.4 ± 0.97	1.57 ± 0.02	2.0–4.0	10YR 3/4
	0.42–1.00	15.7	35.2	48.8	0.3	11.5 ± 0.13	18.25 ± 0.99	3.5 ± 0.58	1.77 ± 0.02	<1.0	10YR 5/3
C	0.00–0.28	6.1	44.9	48.7	0.3	8.1 ± 0.1	21.6 ± 1.0	8.4 ± 0.9	1.64 ± 0.02	2.0–4.0	10YR 3/3
	0.28–1.00	12.6	39.3	47.8	0.3	10.38 ± 0.1	15.9 ± 0.4	7.83 ± 0.2	1.75 ± 0.01	<1.0	10YR 4/6
R	0.00–0.35	0.3	1.8	89.8	8.1	6.4 ± 0.00	24.0 ± 0.83	8.2 ± 0.30	1.63 ± 0.00	1.0–2.0	10YR 4/2
	0.35–1.00	0.0	0.5	99.5	0.0	0.9 ± 0.00	34.1 ± 0.45	12.5 ± 1.59	1.39 ± 0.03	0.0	2.5 Y 5/4

Image Processing and Statistical Analyses

All image processing was done using Photoshop CS6 (Adobe Systems Inc.). Prior to the processing of photographs, we applied a photogrammetric rectification. Then, the photographs were edited, adjusting contrast and brightness. Finally, stained areas were isolated from unstained areas manually by visual inspection, and the results were presented in a binary (black and white) image (Nobles et al., 2010).

The pixels of stained and unstained areas from each profile section were counted in squares of 0.05 × 0.05 m and pixelwise per row in the downward direction of the soil profile for further statistical analysis.

Since the dye coverages were not normally distributed, differences of stained areas between individual soil profiles were analyzed using a Mann–Whitney U-test.

We calculated vertical and horizontal semivariograms by means of tracer coverage. Vertical semivariograms were calculated by using dye coverage mean values of the eight excavated soil profiles at each site. Horizontal semivariograms were calculated depthwise by taking all values of the eight profiles of one depth (10-cm increments) representing one horizontal plane perpendicular to the soil profile.

The empirical semivariogram cloud was calculated by the following equation:

$$\gamma(h)=\frac{1}{2n(h)}\sum_{i=1}^{n(h)}\left[Z(x_i)-Z(x_j)\right]^2$$

where x_i and x_j are the locations of two measurement spots, $n(h)$ is the set of all pairwise Euclidean distances, and Z is the value of the stained area at the spatial locations x_i and x_j. The locations of the measurement spots were derived from the center of each 0.05 × 0.05 m square in the processed images.

We fitted linear and spherical semivariogram models to the empirical semivariogram cloud according to the following equations (spherical semivariogram model):

$$\gamma(h)=c_0+c\left(\frac{3h}{2a}-\frac{h^3}{2a^3}\right), \quad for\ 0<h\le a$$

$$\gamma(h)=c_0+c, \quad for\ h>a$$

where h is the Euclidean distance, c_0 is the nugget, c_0+c is the sill, and a is the range of the semivariogram. The theoretical semivariogram models were validated by the minimized sum of squares.

The semivariogram is a quantitative description of spatial patterns in the soil. It provides information on spatial dependencies of measured parameters and is, thereby, a prerequisite for the justified interpolation and mapping of soil properties (Burgess and Webster, 1980). Semivariograms have rarely been used to describe spatial variability of soil dye patterns (Liu and Lennartz, 2015). The semivariogram allows one to limit the spatial extent of autocorrelation, which is helpful in interpreting flow and transport domains in soils.

Results and Discussion

Observed Dye Patterns

Profound differences in the relation of stained and unstained areas could be observed for BB and TiO_2 (Fig. 1 and 2). The average BB-stained area, as calculated from eight soil profiles, was 0.14, 0.15, and 0.12 m^2 for the sites S, C, and R, respectively, which corresponds to a relative coverage of 29, 31, and 24%.

For the upper soil horizon (0.3 m) we calculated mean BB-dye coverages of 0.12 m^2 (57%) for all three sites. The difference in dye coverage between topsoil (0–0.3 m) and subsoil (0.3–0.7 m) was significant for all three sites and all profiles ($p < 0.001$). The stained area in the lower 0.4 m of the soil profiles was 0.02, 0.02, and 0.004 m^2 at the sites S, C, and R, respectively, which corresponds to a relative coverage of 7, 7, and 1% (Fig. 3).

Brilliant Blue passed the upper soil horizons in a broad front at all sites, whereas the compacted subsoil with higher bulk densities restricted the transport of BB to preferential flow pathways. At sites S and C, subsoil-related preferential transport patterns were evident. The macropore system consisted of earthworm burrows and root channels. At site R, however, BB did not pass the A horizon within 24 h after tracer application. In contrast, BB reached the lower boundary (0.7 m) of all soil profiles at sites S and C.

The overall mean area covered by TiO_2 tracer was lower by the factor ten compared with BB, with 0.005, 0.008, and 0.0 m^2 for

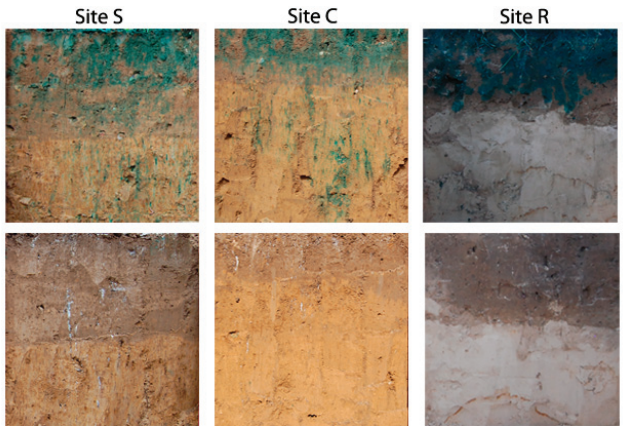

Fig. 1. Sample images of stained soil profiles. The upper row shows Brilliant Blue, while the lower row shows TiO_2.

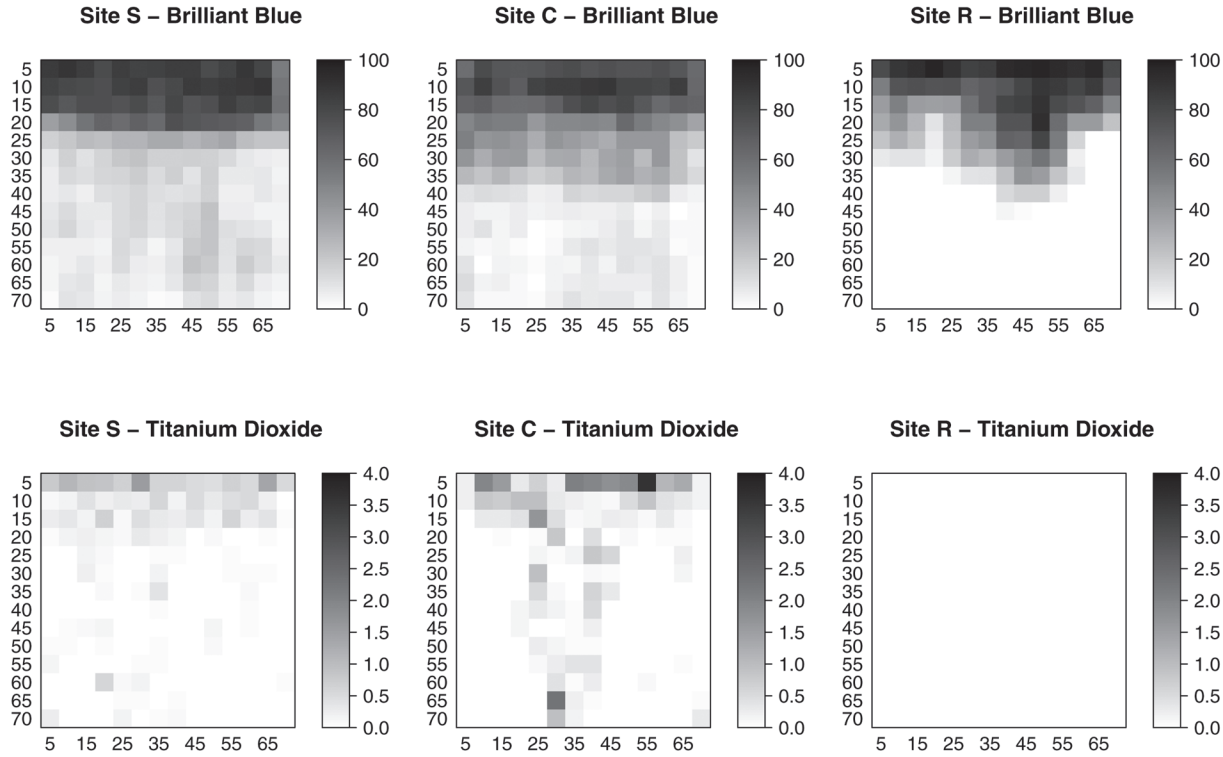

Fig. 2. Mean coverage (%) of dye tracer, as determined in 5 by 5 cm squares of all soil profiles per site (n = 8). Note the differences in gray scaling for Brilliant Blue and titanium dioxide.

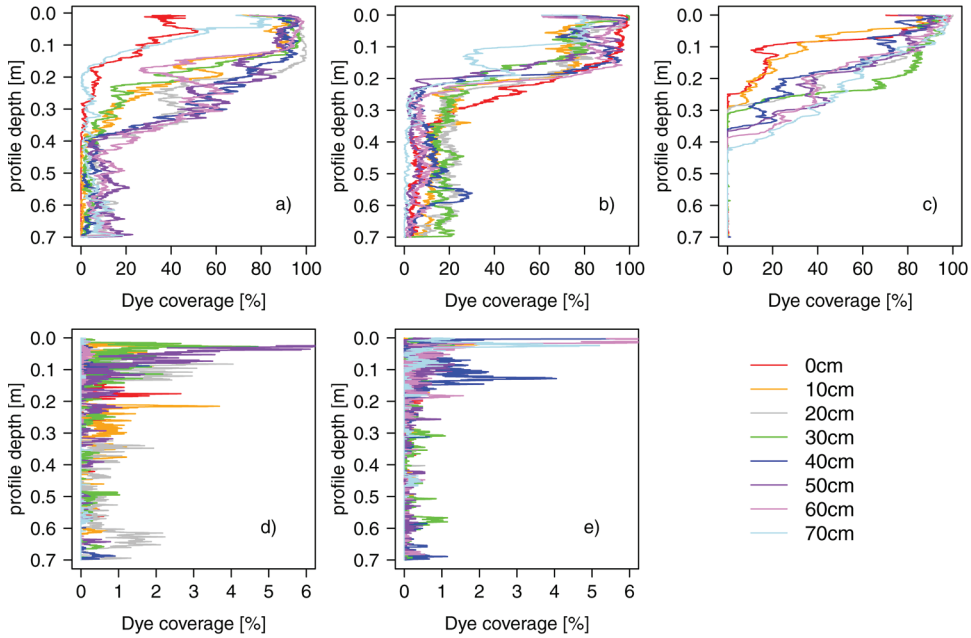

Fig. 3. Vertical dye coverages of each site and each tracer per soil profile with (a) site S (Brilliant Blue), (b) site C (Brilliant Blue), (c) site R (Brilliant Blue), (d) site S (TiO_2), and (e) site C (TiO_2). There is no graph for TiO_2 at site R, because no tracer was found in the soil profiles.

the sites S, C, and R, respectively, which corresponds to a relative coverage of 1, 1, and 0% (Fig. 1). At site R, no tracer at all was found in the soil profiles. The upper soil horizons (0–0.3 m) were covered with TiO_2 dye on an area of 8.95×10^{-4} and 5.89×10^{-4} m^2 at sites S and C, respectively. In the subsoil (0.3–0.7 m) the mean coverage was 7.23×10^{-4} and 4.59×10^{-4} m^2 at sites S and C, respectively. This corresponds to relative coverages of <1%.

The dye photographs clearly demonstrate the differences in transport between TiO_2 and BB at sites S and C. Titanium(IV) oxide is exclusively transported through singular macropores; matrix transport is not visible (Fig. 4). In contrast, BB is transported by matrix flow, as indicated by the homogeneous coverage of the soil and at greater depths through the secondary pore system, as originating from aggregation and biological activity (root and earthworm channels). This has also been observed by Nobles et al. (2010).

Tillage of the upper soil horizon leads to a great proportion of highly accessible and equally distributed pores, allowing the transport of water and BB, which results in a more-or-less

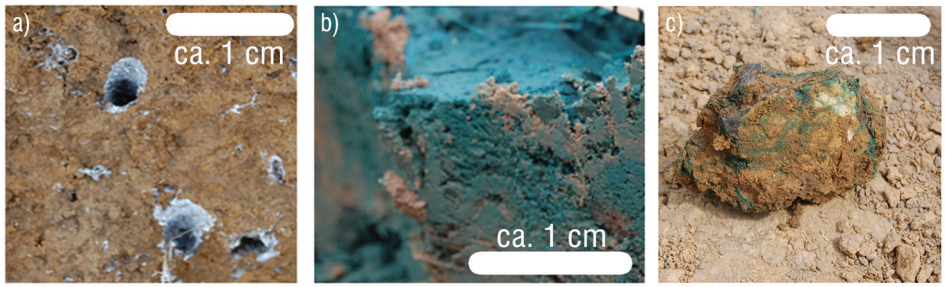

Fig. 4. Horizontal cut through soil profiles at site S. Figure (a) shows the transport of TiO_2 through earthworm channels (0.4-m depth), (b) shows matrix transport of Brilliant Blue (BB) in the topsoil (0.2-m depth), and (c) shows transport of BB through the interaggregate pore system.

homogeneously stained A horizon (Yasuda et al., 2001). An increasing bulk density and clay content in the B horizon facilitate the structuring and formation of larger aggregates, which result in a more pronounced separation of the pore space in an inter- and intra-aggregate domain. As a consequence, a distinct pattern of preferential pathways are established. In contrast to BB, TiO_2 is exclusively transported through singular macropores (e.g., earthworm channels) across the soil profile, also in the A horizon. It was interesting to see that TiO_2 did not travel through large cracks, as they originated from aggregation.

The results indicate that BB, in contrast to TiO_2, is transported through aggregate interfaces (Fig. 4c), root channels (Fig. 1), and other macropores (Fig. 1) of biological origin, which confirms earlier observations (Nobles et al., 2004). Similar to the results from this study, Yasuda et al. (2001) observed that applying BB under ponding conditions stains up to 100% of the upper part of a clay soil profile and follows preferential pathways in the subsoil. The authors estimated that only 10 to 20% of the cracks in the observed prismatic clay were active pore space and accessible for preferential transport. In more coarse-textured soils, they observed fuzzy dye patterns and deduced dispersive transport mechanisms. Preferential flow of BB solution in compact clay and loam soils has also been shown by Hardie et al. (2011), Chyba et al. (2013), and Etana et al. (2013).

Dye tracer studies regarding TiO_2 are rare. Liu and Lennartz (2015) investigated the effect of applying TiO_2 as a tracer in degraded peat soils in northeastern Germany. They found that TiO_2 is transported preferentially and, in contrast to bromide as a conservative tracer and solute, has limited or no access to the fine pore system. It can be assumed that, in our study, BB behaved as a solute and was subjected to lateral transport by diffusion, in addition to convective–dispersive mechanisms. Although diffusion in soils is in general lower as compared with a free solution, the entrance of BB into the fine pore system is possible and could be confirmed by photo documentation (Fig. 1 and 4c). In contrast, diffusion of TiO_2 is negligible, and access to the fine pore system is hindered because of the weight and size of the particles. We presume that, with increasing colloid size of the tracer suspension, the amount of active pore space decreases in the soil.

Spatial Distribution of Dye Tracer in the Soil Profiles

We calculated empirical semivariograms and fitted theoretical linear and spherical models to the data to assess the spatial variability of the dye patterns. Vertical semivariogram models indicate a strong spatial variability across all sites for both BB and TiO_2 (Fig. 5). The semivariograms do not reach a sill until the maximum distance. Zero nuggets were calculated for all three BB semivariograms. This implies that the total stained area decreases with increasing depth, even outreaching the observed profile depth. This can be attributed to preferential flow through the secondary pore system (BB) and through singular macropores (particle transport, BB), as has often been observed in dye tracer studies (Weiler and Flühler, 2004; Kasteel et al., 2005; Nobles et al., 2010; Liu and Lennartz, 2015).

The semivariograms for the horizontal plane indicate a smaller spatial variability compared with the vertical semivariograms and also show a strong spatial dependence of dye coverage in the horizontal direction over short distances. This result suggests that individual and continuous pores, such as well-confined interaggregate spaces (BB) or biopores (BB + TiO_2), are the prime flux and particle transport domain, rather than 'flux fingers,' for instance. A sill was reached in the theoretical semivariogram models at almost all horizontal cross-sections for both BB and TiO_2 (Fig. 6).

Yasuda et al. (2001) showed that the spatial dependence in the horizontal direction is larger than in the vertical direction. This can be interpreted as a geostatistical expression of preferential flow through the soil profile. The effect of earthworm and root channels appears higher in the vertical direction than in the horizontal direction.

The low nuggets in the horizontal semivariograms suggest that the spatial extent of the processes of vertical particle-facilitated transport can be mapped on the pedon scale.

Influence of Soil Texture on Dye Patterns

The results reveal a small but statistically significant positive relationship between the clay content and TiO_2-stained area for the topsoil and the subsoil ($R^2 = 0.24$, $p < 0.05$ for topsoil and $R^2 = 0.2$, $p < 0.05$ for subsoil; linear regression model). Furthermore, we found a significant relationship between

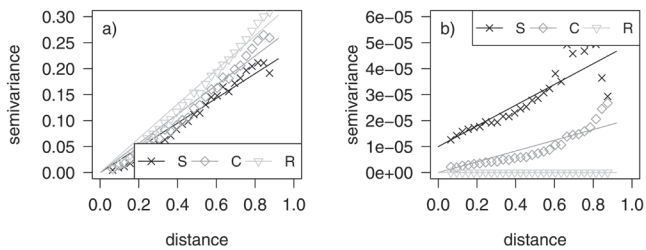

Fig. 5. Vertical empirical semivariogram clouds and fitted linear (Brilliant Blue, panel a) and Gaussian (TiO_2, panel b) semivariogram models for the three sites and both tracers.

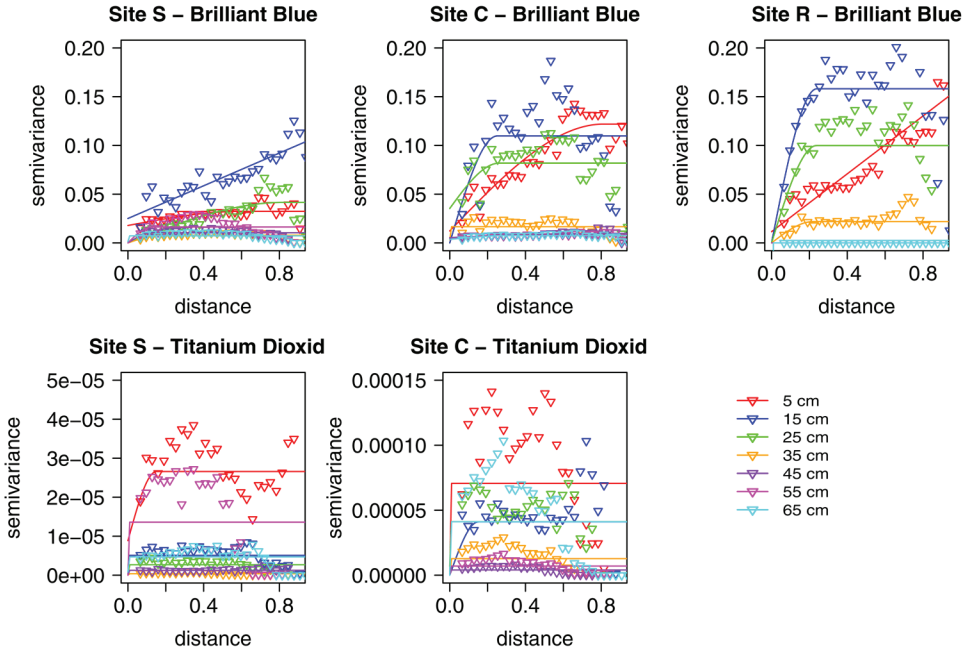

Fig. 6. Horizontal empirical semivariograms and fitted spherical semivariogram models for different depths in 10-cm steps. Note the varying *y*-axis.

dye coverage of TiO_2 and silt content ($R^2 = 0.29$, $p < 0.05$ for topsoil and $R^2 = 0.26$, $p < 0.05$ for subsoil; linear regression model). On the other hand, a combination of both clay and silt content gave no significant model. However, neither the pore size distribution, nor the content of sand, has any effect on the stained area of the soil.

At site R, we found a sandy soil with a lack of clay minerals and organic matter. Consequently, the soil particles are predominantly unaggregated and loose; no soil structure forming a secondary pore system has developed. In contrast, at sites S and C, an advanced pedogenesis with nuanced manifestation of soil horizons can be expected. This can also be seen in the formation of a solid soil structure, the higher bulk densities, and the stable pore system.

We assume that higher clay and silt contents result in a more structured soil, which leads to a pronounced secondary pore space and, hence, to a higher potential for the (preferential) transport of solutes and colloids. Organic matter content, which was greater at sites C and S as compared with site R, may also play an important role in the formation and stability of soil peds (Chaplot and Cooper, 2015). De Jonge et al. (2004) also found the clay content and the continuity of large macropores as an explanation for enhanced particle-facilitated transport.

Brilliant Blue is an extensively studied dye tracer, but studies on the influence of soil characteristics on the obtained dye patterns are less frequent. Flury et al. (1994) found that structured soils were penetrated deeper by BB than unstructured soils, which well reflects our results with structured soils at site S and C and the unstructured soil at site R.

We believe that the higher clay content causes temporal, resistant, singular biogene macropores that can transport the TiO_2 suspension through the soil, while in loose-bedded soils, earthworm holes are not persistent and soil macropores only allow very limited access of colloidal TiO_2.

Suitability of TiO_2 as a Colloid Dye Tracer

Several studies on the transport of colloids are documented in the literature, whereby particle sizes in the range of 0.1 to 1.0 μm were considered, which was likewise the dominant range of TiO_2 particles used in our study (Makris et al., 2006, >0.45 μm; VandeVoort et al., 2013, <1 μm; Knappenberger et al., 2014, 0.22 μm). Particle sizes of clay minerals and metal oxides are similar to the sizes of the TiO_2 particles presented here. Makris et al. (2006) stated that iron hydroxides are an important fraction of potentially mobile soil colloids. We thus conclude that TiO_2 is a useful substance for the indication of potential pathways of colloids in soils. This assumption is supported by comparable densities of TiO_2 and different metal oxides. Cey et al. (2009), however, found that the colloid species do not influence transport to a greater degree than the flow system itself and concluded that even soluble dye tracers like BB are a reasonable surrogate for colloid distributions in the vadose zone. The comparison of TiO_2 and BB images, nonetheless, revealed that transport pathways of soluble and colloidal substances are not necessarily identical.

Conclusions

We studied the visualization potential of particle facilitated transport by using TiO_2 as a tracer in mineral soils. The results revealed that both the solution (BB), as well as the suspension (TiO_2), follow preferential pathways; TiO_2 is, however, exclusively transported in singular macropores, rather than along soil ped interfaces. They also reveal that there is a significant trend that greater clay and even silt contents cause a higher TiO_2 coverage of the soil profile, indicating a more pronounced leaching potential for particles in structured soils. Based on our findings and the observed differences in transport patterns between BB and TiO_2, we conclude that TiO_2 is suitable for the visualization of colloid pathways in the soil.

The observations made emphasize the importance of the active pore system in contrast to the overall pore space for preferential transport of colloids through soils. To date, the spatial

distribution of particle pathways in the soil profile and its large spatial variability is not well understood and calls for further research. In a next step, dye tracing should be combined with a quantification of solute and particle transport across a flux plane to allow the derivation of quantitative indices from the stained soil profiles using TiO_2. Furthermore, since there are hints in the literature, different regimes of rainfall and initial soil moisture contents should be considered in particle tracer studies, as those might influence colloid transport and mobilization.

Acknowledgments

We kindly acknowledge the help of our field workers Christian Möller, Robert Schmidtke, and Stefan Kopperschmidt. We would likewise thank Dr. Andreas Bauwe and Evelyn Bolzmann for laboratory analysis regarding soil physical properties. The authors gratefully acknowledge the German Federal Ministry of Education and Research (BMBF) for funding the BonaRes project InnoSoilPhos (No. 031A558).

References

Burgess, T.M., and R. Webster. 1980. Optimal interpolation and isarithmetic mapping of soil properties. J. Soil Sci. 31:333–341. doi:10.1111/j.1365-2389.1980.tb02085.x

Cey, E.E., D.L. Rudolph, and J. Passmore. 2009. Influence of macroporosity on preferential solute and colloid transport in unsaturated field soils. J. Contam. Hydrol. 107:45–57. doi:10.1016/j.jconhyd.2009.03.004

Chaplot, V., and M. Cooper. 2015. Soil aggregate stability to predict organic carbon outputs from soils. Geoderma 243-244:205–213. doi:10.1016/j.geoderma.2014.12.013

Chyba, J., M. Kroulik, J. Lev, and F. Kumhála. 2013. Influence of soil cultivation and farm machinery passes on water preferential flow using brilliant blue dye tracer. Agron. Res. 11:25–30.

Cnudde, V., B. Masschaele, M. Dierick, J. Vlassenbroeck, L. van Hoorebeke, and P. Jacobs. 2006. Recent progress in X-ray CT as a geosciences tool. Appl. Geochem. 21:826–832. doi:10.1016/j.apgeochem.2006.02.010

Daniel, T.C., A.N. Sharpley, D.R. Edwards, R. Wedepohl, and J.L. Lemunyon. 1994. Minimizing surface water eutrophication from agriculture by phosphorous management. J. Soil Water Conserv. 49:30–38.

de Jonge, L.W., P. Moldrup, G.H. Rubæk, K. Schelde, and J. Djurhuus. 2004. Particle leaching and particle-facilitated transport of phosphorus at field scale. Vadose Zone J. 3:462–470. doi:10.2113/3.2.462

Deutsches Institut für Normung. 2011. Soil, investigation and testing—Determination of grain-size distribution. DIN 18123. (In German.) Deutsches Institut für Normung, Berlin, Germany.

Etana, A., M. Larsbo, T. Keller, J. Arvidsson, P. Schjønning, J. Forkman, and N. Jarvis. 2013. Persistent subsoil compaction and its effects on preferential flow patterns in a loamy till soil. Geoderma 192:430–436. doi:10.1016/j.geoderma.2012.08.015

Flury, M., and H. Flühler. 1995. Tracer characteristics of Brilliant Blue FCF. Soil Sci. Soc. Am. J. 59:22–27. doi:10.2136/sssaj1995.03615995005900010003x

Flury, M., H. Flühler, W.A. Jury, and J. Leuenberger. 1994. Susceptibility of soils to preferential flow of water: A field study. Water Resour. Res. 30:1945–1954. doi:10.1029/94WR00871

Frazier, T.P., C.E. Burklew, and B. Zhang. 2014. Titanium dioxide nanoparticles affect the growth and microRNA expression of tobacco (*Nicotiana tabacum*). Funct. Integr. Genomics 14:75–83. doi:10.1007/s10142-013-0341-4

Germán-Heins, J., and M. Flury. 2000. Sorption of Brilliant Blue FCF in soils as affected by pH and ionic strength. Geoderma 97:87–101. doi:10.1016/S0016-7061(00)00027-6

Hardie, M.A., W.E. Cotching, R.B. Doyle, G. Holz, S. Lisson, and K. Mattern. 2011. Effect of antecedent soil moisture on preferential flow in a texture-contrast soil. J. Hydrol. 398:191–201. doi:10.1016/j.jhydrol.2010.12.008

Heathwaite, L., P.M. Haygarth, R. Matthews, N. Preedy, and P. Butler. 2005. Evaluating colloidal phosphorus delivery to surface waters from diffuse agricultural sources. J. Environ. Qual. 34:287–298. doi:10.2134/jeq2005.0287

IUSS Working Group WRB. 2015. World reference base for soil resources 2014, update 2015: International soil classification system for naming soils and creating legends for soil maps. World Soil Resour. Rep. 106. FAO, Rome.

Jacobsen, O., P. Moldrup, C. Larsen, L. Konnerup, and L. Petersen. 1997. Particle transport in macropores of undisturbed soil columns. J. Hydrol. 196:185–203. doi:10.1016/S0022-1694(96)03291-X

Janssen, M., and B. Lennartz. 2008. Characterization of preferential flow pathways through paddy bunds with dye tracer tests. Soil Sci. Soc. Am. J. 72:1756–1766. doi:10.2136/sssaj2008.0032

Jiang, X., R. Bol, S. Willbold, H. Vereecken, and E. Klumpp. 2015. Speciation and distribution of P associated with Fe and Al oxides in aggregate-sized fraction of an arable soil. Biogeosciences 12:6443–6452. doi:10.5194/bg-12-6443-2015

Kasteel, R., M. Burkhardt, S. Giesa, and H. Vereecken. 2005. Characterization of field tracer transport using high-resolution images. Vadose Zone J. 4:101–111. doi:10.2113/4.1.101

Kasteel, R., H.-J. Vogel, and K. Roth. 2002. Effect of non-linear adsorption on the transport behaviour of Brilliant Blue in a field soil. Eur. J. Soil Sci. 53:231–240. doi:10.1046/j.1365-2389.2002.00437.x

Knappenberger, T., M. Flury, E.D. Mattson, and J.B. Harsh. 2014. Does water content or flow rate control colloid transport in unsaturated porous media? Environ. Sci. Technol. 48:3791–3799. doi:10.1021/es404705d

Kodešová, R., K. Němeček, A. Žigová, A. Nikodem, and M. Fér. 2015. Using dye tracer for visualizing roots impact on soil structure and soil porous system. Biologia 70:1439–1443. doi:10.1515/biolog-2015-0166

Liu, H., and B. Lennartz. 2015. Visualization of flow pathways in degraded peat soils using titanium dioxide. Soil Sci. Soc. Am. J. 79:757–765. doi:10.2136/sssaj2014.04.0153

Long, T.C., N. Saleh, R.D. Tilton, G.V. Lowry, and B. Veronesi. 2006. Titanium dioxide (P25) produces reactive oxygen species in immortalized brain microglia (BV2): Implications for nanoparticle neurotoxicity. Environ. Sci. Technol. 40:4346–4352. doi:10.1021/es060589n

Makris, K.C., J.H. Grove, and C.J. Matocha. 2006. Colloid-mediated vertical phosphorus transport in a waste-amended soil. Geoderma 136:174–183. doi:10.1016/j.geoderma.2006.03.027

McGechan, M.B., and D.R. Lewis. 2002. Transport of particulate and colloid-sorbed contaminants through soil, part 1: General principles. Biosystems Eng. 83:255–273. doi:10.1006/bioe.2002.0125

Morris, C., S.J. Mooney, and S.D. Young. 2008. Sorption and desorption characteristics of the dye tracer, Brilliant Blue FCF, in sandy and clay soils. Geoderma 146:434–438. doi:10.1016/j.geoderma.2008.06.021

Nobles, M.M., L.P. Wilding, and H.S. Lin. 2010. Flow pathways of bromide and Brilliant Blue FCF tracers in caliche soils. J. Hydrol. 393:114–122. doi:10.1016/j.jhydrol.2010.03.014

Nobles, M.M., L.P. Wilding, and K.J. McInnes. 2004. Pathways of dye tracer movement through structured soils on a macroscopic scale. Soil Sci. 169:229–242. doi:10.1097/01.ss.0000126838.81093.20

Rogasik, H., J.W. Crawford, O. Wendroth, I.M. Young, M. Joschko, and K. Ritz. 1999. Discrimination of soil phases by dual energy x-ray tomography. Soil Sci. Soc. Am. J. 63:741–751. doi:10.2136/sssaj1999.634741x

Sharpley, A.N., S.C. Chapra, R. Wedepohl, J.T. Sims, T.C. Daniel, and K.R. Reddy. 1994. Managing agricultural phosphorous for protection of surface waters: Issues and options. J. Environ. Qual. 23:437–451. doi:10.2134/jeq1994.00472425002300030006x

Sharpley, A.N., and J.K. Syers. 1979. Phosphorus inputs into a stream draining an agricultural watershed. Water Air Soil Pollut. 11:417–428. doi:10.1007/BF00283433

Soil Survey Staff. 1999. Soil taxonomy: A basic system of soil classification for making and interpreting soil surveys. 2nd ed. USDA–NRCS Agric. Handb. 436. U.S. Gov. Print. Office, Washington, DC.

Stamm, C., H. Flühler, R. Gächter, J. Leuenberger, and H. Wunderli. 1998. Preferential transport of phosphorus in drained grassland soils. J. Environ. Qual. 27:515–522. doi:10.2134/jeq1998.00472425002700030006x

VandeVoort, A.R., K.J. Livi, and Y. Arai. 2013. Reaction conditions control soil colloid facilitated phosphorus release in agricultural Ultisols. Geoderma 206:101–111. doi:10.1016/j.geoderma.2013.04.024

Weiler, M., and H. Flühler. 2004. Inferring flow types from dye patterns in macroporous soils. Geoderma 120:137–153. doi:10.1016/j.geoderma.2003.08.014

Weir, A., P. Westerhoff, L. Fabricius, K. Hristovski, and N. von Goetz. 2012. Titanium dioxide nanoparticles in food and personal care products. Environ. Sci. Technol. 46:2242–2250. doi:10.1021/es204168d

Yasuda, H., R. Berndtsson, H. Persson, A. Bahri, and K. Takuma. 2001. Characterizing preferential transport during flood irrigation of a heavy clay soil using the dye Vitasyn Blau. Geoderma 100:49–66. doi:10.1016/S0016-7061(00)00080-X